Manuscript title:

Proteomic responses of HepG2 cell monolayers and 3D spheroids to selected hepatotoxins

Manuscript ID: TOXLET_2018_90

Submission date: 25/08/2018

Revision date: 28/09/2018

Authors and affiliations:

Tracey Hurrell[a,l] (tracey.hurrell@ki.se)

Kathryn S. Lilley[b] (k.s.lilley@bioc.cam.ac.uk)

Allan Duncan Cromarty[a] (duncan.cromarty@up.ac.za)

[a]Department of Pharmacology, Faculty of Health Sciences, School of Medicine,

University of Pretoria, Private Bag X323, Arcadia, 0007, South Africa

[b]Cambridge Centre for Proteomics, Department of Biochemistry,

University of Cambridge, Tennis Court Road, Cambridge CB2 1QR, United Kingdom

[l] Section of Pharmacogenetics, Department of Physiology and Pharmacology,

Karolinska Institutet, Solnavägen 9, 171 65 Solna, Sweden

Correspondence:

Tracey Hurrell
Section of Pharmacogenetics
Department of Physiology and Pharmacology
Karolinska Institute
Solnavägen 9
171 65 Solna, Sweden
tracey.hurrell@ki.se
traceyhurrell@hotmail.com
+46-(0)8-524 877 62

Financial support:

National Research Foundation Thuthuka Funding Scheme (Grant No. 87880.)

UK Commonwealth Split-site Scholarship (ZACS-2014-653)

Commonwealth, European and International Cambridge Trust Scholarship

Abstract

Despite the importance of hepatotoxicity testing in the development of new potential pharmaceuticals, standardized methods for preclinical *in vitro* hepatotoxicity is complicated by the perceived adequacy of approach, diversity of origin of cells, and the ability to retain a satisfactory hepatocellular phenotype. Additionally, the confidence with which cells mimic *in vitro* hepatocytes is dictated by the spatial dynamics of the cell culture microenvironment. This study sought to compare the proteome of conventional monolayer cultures of an immortalized hepatocyte cell line (HepG2) with more complex three-dimensional spheroid cultures to ascertain whether changes in culture technique better mimic the phenotype of hepatocytes and thereby improve responses to *in vivo* hepatotoxins. The proteome was assayed using isobaric tagging from six independent experiments, yielding relative quantitation of over 4600 proteins per multiplexed set. Approximately 34% of proteins present in all replicates differed between monolayer and 3D spheroid cultures. These data suggest that the cellular transition from exponential to equilibrium growth phases is inconsistent across biological replicates during spheroid formation which then variably alters the proteome from a stable phenotype in monolayers. Continuous exposure to hepatotoxins, did not implicate specific subsets of proteins in describing the associated mechanisms of toxicity of each drug. However, dynamic changes in the HepG2 cells cultured as 3D spheroids were uncovered. These data suggest that the duration of spheroid culture could be essential to reconcile the differences observed in the spheroid proteome to achieve reproducible proteomic transitions to a stable 3D spheroid phenotype.

Keywords: HepG2 cells, hepatotoxicity, spheroids, proteomic assay

1. Introduction

Merging the "Paracelsus doctrine" with modern pharmaceutical safety regulations necessitates the evaluation of safety thresholds in drug research and development (Kinter *et al.*, 2002; Niles *et al.*, 2009; Redfern *et al.*, 2002). Despite numerous preclinical *in vivo* models to study pathologies and liver toxicities (Bhakuni *et al.*, 2016), ethical considerations and concerns over extrapolation from preclinical data intensify the pressure facing preclinical research (Cai *et al.*, 2012). In addition, a paradigm shift for human toxicity testing urges that mechanistic elucidation and identification of adverse drug reactions (ADRs) be pathway driven. These assays must be conducted using human-derived cells to ensure applicable phenotypic responses by the test system (Krewski *et al.*, 2009). Safety testing strives to improve drug safety profiles, reduce unrecoverable costs from clinical failure and promote market longevity (Feng *et al.*, 2014; Kola *et al.*, 2004). However, drug withdrawal remains a burden for the pharmaceutical industry (Kola & Landis, 2004) with historically highly publicised drug withdrawals including Iproniazid (1961)(Kline, 1970), Bromfenac (1998)(Hunter *et al.*, 1999), to the more recent Troglitazone (2000)(Gale, 2006) and Fasiglifam a first in-class GPR40 agonist (2014)(Kaku *et al.*, 2015). Amongst others, hepatotoxicity is one contributor to investigational new drug failure and a major justification for postmarketing regulatory decisions including black-box warnings and drug withdrawals (Cai *et al.*, 2012). The need for harmonized approaches in preclinical hepatotoxicity research have been emphasized over the past decades, but the complexity involved limits the implementation of definitive recommendations (Hughes, 2008). Highly predictive *in vitro* hepatotoxicity assays using human liver models will continually be required for decision making in the pharmaceutical industry. Innovative models continue to emerge which make use of functional primary human hepatocytes (Bell *et al.*, 2016; Koyama *et al.*, 2018; Rebelo *et al.*, 2017), hepatocytes derived from induced pluripotent stem cells (Heidariyan *et al.*, 2018; Kamei *et al.*, 2017) and immortalized hepatic cell lines (Mueller *et al.*, 2014; Ramaiahgari *et al.*, 2014). Technological advancements are improving *in vivo* applicability, in some part, due to the use of a variety of three-dimensional (3D) cell culture strategies (Griffith *et al.*, 2006; Lauschke *et al.*, 2016).

The rapidly emerging field of 3D culture comprises static and perfused systems which vary in complexity to include sandwich cultures, spheroid systems, hollow fiber 3D bioreactors and organ-on-a-chip platforms (Griffith *et al.*, 2006; Lauschke *et al.*, 2016). Cultured cellular aggregation under gravity enforcement, commonly known as hanging drop cultures, have been used to successfully produce scaffold-free spheroids (Foty, 2011), but were technically limited until commercially available resources (InSphero®, 3D Biomatix Inc®) improved their application. Hanging drop cultures are now used to produce 3D spheroids including intestinal organoids (Panek *et al.*, 2018), adipose spheroids (Klingelhutz *et al.*, 2018) and immortalized HepG2 cell spheroids (Shah *et al.*, 2018). Immortalized hepatocytes have been reported to exhibit varied phenotypic characteristics and functional properties (Duret *et al.*, 2007). Despite known metabolic limitations, guidelines for hepatotoxicity testing generally do not preclude the use of HepG2 cells and therefore remain an attractive tool for researchers (Paech *et al.*, 2018; Ramirez *et al.*, 2018; Shah *et al.*, 2018; Yang *et al.*, 2018). Spheroids and other 3D cultures alter the dynamic equilibrium established in cells and are suggested to improve the mimicry of *in vivo* counterparts (Ramaiahgari *et al.*, 2014; Wrzesinski *et al.*, 2014). However, the phenotypic changes are inconsistent as not only does the cellular source influence spheroid characteristics but fundamental features like medium volume in hanging-drops (Hurrell, Ellero*, et al.*, 2018) and spheroid separation distance in micro-patterned chip cultures modulate spheroid properties (Miyamoto *et al.*, 2018). HepG2 and HepaRG cell lines have been used to identify DILI compounds consistent with reported clinical mechanisms (Saito *et al.*, 2016) which warrants continued improvement of these approaches. Deeper insight into the molecular and cellular toxicological findings is essential to recapitulating biological relevance (Ahuja *et al.*, 2014) and is dependent on the correct combination of cell type and spheroid culture. As HepG2 cells continue to be of use in hepatotoxicity testing, a detailed proteomic investigation was conducted to identify whether culturing these cells as 3D spheroids improved their phenotype and overall capacity to provide meaningful proteomic signatures of hepatotoxicity.

2. Materials and methods

2.1 HepG2 3D spheroid cultures

HepG2 3D spheroids were generated as previously described (Hurrell, Segeritz*, et al.*, 2018). Human hepatocellular carcinoma cells, HepG2 (CHG2-C, Cellonex; South Africa), were cultured in EMEM supplemented with 10% foetal bovine serum, 1% penicillin-streptomycin (10 000 U/ml penicillin, 10 000 µg/ml streptomycin) and 2 mM L-glutamine. Spheroids were generated using the hanging—drop method (Perfecta3D® 96-well plate: 3D Biomatrix; Michigan, USA) by seeding $1x10^4$ cells in 45 µl medium. Plates were incubated at 37°C with 5% CO_2 with partial medium exchange (20 µl) performed every alternate day. Live-dead staining of spheroids with fluorescein diacetate and propidium iodide, to confirm viability, was conducted as previously described (Hurrell, Ellero*, et al.*, 2018).

2.2 Cell enumeration in HepG2 monolayers

HepG2 cells ($2x10^4$ cells/well) were seeded, and left to adhere overnight, in round-bottomed 96-well plates. Cells were exposed to *in vivo* hepatotoxins, Bromfenac, Ketoconazole, and Troglitazone (seven half-log concentrations: 0.1-100 µM), as well as non-hepatotoxic Diphenhydramine and enumerated using a modified sulforhodamine B (SRB) assay (Vichai *et al.*, 2006).

Hepatotoxic drugs were selected from different therapeutic classes based on their potential for drug-induced liver injury (DILI) concern. Criteria for hepatotoxic drugs included being in the top 10 therapeutic classes of highest DILI concern (Chen *et al.*, 2011), along with having been withdrawn from the market for oral administration (Supplementary data II: Table 1). Following exposure for 72 hours, cells were fixed with the addition of 50 µl of 50% trichloroacetic acid and incubated overnight at 4°C. Fixed cells were stained with 100 µl SRB solution (0.057% in 1% acetic acid) for 30 minutes, gently washed with 1% acetic acid to remove staining solution and solubilised with 200 µl Tris-base solution (10 mM; pH 10.5). Absorbance was measured at a dual wavelength of 510 nm and 630 nm using an Elx800 Bio-Tek microplate reader.

2.3 In vitro hepatotoxicity screening

Six end-point assays were conducted simultaneously (van Tonder, 2011), after 24 and 72 hours exposure. HepG2 cells ($2x10^4$ cells/well) were cultured overnight in opaque flat-bottomed 96-well plates prior to exposure to each drug (five half-log concentrations: 1-100 µM). Assays, further detailed in Supplementary data II: Table 2, included cell enumeration (CV: SRB), generation of reactive oxygen species (ROS: 10 µM H_2-DCF-DA), intracellular reduced glutathione (GSH: 16 µM monochlorobimane), mitochondrial membrane potential (MMP: 10 µM JC-1), intracellular fatty acid accumulation (FAA or steatosis: 1 µM nile red) and apoptosis (caspase-3/7: 4 µM Ac-DEVD-AMC). Following incubation with 100 µl of each dye solution in HBSS for 2 hours at 37°C, ROS, GSH, MMP and steatosis were quantified, at their respective excitation and emission wavelengths, using a FLUOstar Optima micro-plate reader. For caspase-3/7 activity, cells were lysed (25 µl; 10 mM HEPES, 5 mM CHAPS, 2 mM EDTA, with 1 mM PMSF and 5 mM β-mercaptoethanol, pH7.4) on ice for 40 minutes. Assay buffer was added (100 µl; 20 mM HEPES, 2 mM EDTA, with 5 mM β-mercaptoethanol and 5 µM Ac-DEVD-AMC) and plates incubated at 37°C for 4 hours. Fluorescence signal was normalized, for non-ratiometric dyes, using the SRB assay.

2.4 Drug exposure, protein harvesting and SDS-PAGE

HepG2 monolayers ($2.5x10^5$ cells/well) in 6-well plates or spheroids ($1x10^4$ cells/well) were seeded and incubated for 4 days after which aggregated spheroids (n=24) were transferred to 6-well plates where they were maintained in suspension by the addition of 0.5% methylcellulose to the culture medium. Cells were exposed to the IC_{20} obtained from the SRB dose-response curve or relative to drug C_{max}. The C_{max} for Bromfenac was calculated based on oral exposure in healthy subjects (8.8 mg/ml (Högger *et al.*, 1993)) and exposed at 25 µM whereas the C_{max} of non-hepatotoxic Diphenhydramine was calculated (66 ng/ml (Blyden *et al.*, 1986) to 92 ng/ml (Gelotte *et al.*, 2018)) and cells exposed at approximately $100xC_{max}$ of 30 µM. Initial exposure was for 72 hours followed by repeated 72 hour exposure to fresh medium containing the same drug concentrations resulting in 6

days of drug exposure with a total of 10 days in culture. Harvested cells, from triplicate seedings, were lysed (10 mM Tris-HCL (pH 8), 1 mM EDTA, 0.5 mM EGTA, 1 % Triton X-100, 0.1% SDS, 0.1% sodium deoxycholate, 140 mM sodium chloride and cOmplete™ protease inhibitor cocktail) on ice for 10 minutes in an ultrasonic bath (Branson, 120W), centrifuged (16 000 *g*; 10 minutes) and the supernatant protein concentration quantified using the bicinchoninic acid assay. Twenty micrograms of protein in Laemmli sample buffer (0.125 M Tris-HCL, 4% SDS, 20% glycerol, 5% β-mercaptoethanol, 0.004% bromophenol blue) was loaded onto Mini-PROTEAN TGX gels (4-15%) and run using a Mini-PROTEAN Tetra System (BioRad Laboratories: Life Science Research Division; California, USA). Gels were stained overnight using Coomassie brilliant blue (0.1% Coomassie brilliant blue R250, 50% methanol, 10% acetic acid), destained (50% methanol, 10% acetic acid) and imaged using a Bio-Rad Doc EZ Imager.

2.5 Protein digestion and tandem-mass tag labelling

Protein (50 µg) from each individual sample was reduced with dithiothreitol (10 mM) for 1 hour at 37°C and alkylated with iodoacetamide (25 mM) for 2 hours at room temperature. Proteins were precipitated with 10 volumes acetone overnight at 4°C, dried and resuspended in 100 µl of 100 mM HEPES (pH 8.5). Samples were digested with sequence-grade modified trypsin (1:40) for 1 hour at 37°C followed by addition of further trypsin (1:40) and overnight digestion at 37°C. Digested peptides were clarified (16 000 *g;* 20 minutes) and the supernatant labelled for 2 hours at room temperature using individual 6-plex TMT reagents (Thermo Fisher Scientific; Massachusetts, USA) resuspended in acetonitrile. Labelling was quenched with the addition of 8 µl of 5% hydroxylamine for 1 hour and further quenched overnight at 4°C with dH_2O. Individual samples were combined (labelling strategy: Supplementary II: Table 3 and 4) and reduced to dryness by vacuum centrifugation.

2.5.1 Solid phase extraction desalting and peptide fractionation

Combined sample peptides were solubilized in 800 µl of 0.1% trifluoroacetic acid (pH 1) and loaded onto a conditioned SepPak C18 cartridge (100 mg). Following desalting with 0.1% TFA and

0.05% acetic acid (pH 3), peptides were eluted in 70% acetonitrile with 0.05% acetic acid, dried and resuspended in 100 µl of 20 mM ammonium formate (pH 10) with 4% acetonitrile. Peptide fractionation was done using a Shimadzu HPLC system coupled to a PDA detector. Peptides were loaded onto an Ascentis C18 HPLC column (150 mm x 4.6 mm, 5 µm) and eluted using a gradient program at a flow rate of 1 ml/minute. An initial 5 minute isocratic low organic mobile phase (5%) of 80% acetonitrile with 20 mM ammonium formate (pH 10) was increased to 75% over 58 minutes with the aqueous mobile phase consisting of 20 mM ammonium formate (pH 10). A rapid step to 100% mobile phase B (80% acetonitrile) was followed by re-equilibrate over a total run time of 75 minutes. Peptides eluting at different retention times were recombined into 12 fractions of similar peptide concentration and resuspended in 2% acetonitrile with 0.1% formic acid.

2.5.2 LC-MS/MS analysis

Samples were analysed at the Central Analytical Facility, University of Stellenbosch using a Dionex Ultimate 3000 RSLCnano LC system coupled to a Fusion Orbitrap Mass Spectrometer (Thermo Fisher Scientific; Massachusetts, USA). Peptides (1 - 2 µg) were loaded onto a C18 trapping column (Thermo Fisher Scientific; 100Å, 5 mm x 300 µm, 5 µm) coupled to a Luna C18 (350 mm x 75 µm, 3.6 µm) analytical column. Samples were loaded onto the trap column from a temperature controlled auto-sampler (7°C) at a flow rate of 15 µl/minute for 5 minutes before eluting onto the analytical column. Peptide separation was performed at 50°C at a flow rate of 500 nl/minute using mobile phase A (2% acetonitrile with 0.1% formic acid) and mobile phase B (100% acetonitrile). A non-linear gradient of 2-50% mobile phase B over 105 minutes was used to separate peptides. Total run time was 120 minutes. Mass-to-charge (m/z) ratios of positively charged ions, with 2 kV spray voltage, was measured in the Orbitrap mass analyser with data acquired in profile mode. Real-time recalibration by correction of m/z shifts for spectra was done using polysiloxane ions at m/z of 371.10024 (positive) and 445.12003 (positive). MS1 scans were performed using the Orbitrap detector (resolution: 120 000) over the scan range 400 - 1650 m/z with AGC target at 2e5 and

maximum Orbitrap injection time of 50 ms. MS2 acquisition was performed using monoisotopic precursor selection for ions with charge states between 2+ and 6+ with an error tolerance of ±10 ppm. Selected precursor ions were fragmented by higher energy collisional dissociation (HCD) set at a normalized collision energy (NCE) of 32.5% with a stepped NCE of 10% in the quadrupole mass analyser which were then excluded from fragmentation once for 30 seconds. Fragment ions were detected, using centroid mode (resolution: 60 000) with the AGC target of 1e5 and maximum injection time of 120 ms.

2.5.3 Data processing, analysis and visualisation

Raw files were converted, with conversion filters of peak picking and a threshold count of 150, to MGF files using ProteoWizard MSConvertGUI (Kessner D, Chambers M et al. 2008). MGF peak lists were searched against a UniProtKB/Swiss-Prot human database (Homo sapiens, Canonical sequence, January 2016, Sequences: 20 194) using SearchGUI version 2.3.1 (Vaudel M, Barsnes H et al. 2011) with X!Tandem, MS-GF+ and Comet search engines. Post-processing of peptide-spectrum matches (PSM) for protein identification was done using Peptide Shaker version 1.7.3 (Vaudel M, Burkhart JM et al. 2015). Search parameters included: minimum and maximum precursor mass of 300 and 900 Da respectively, precursor mass tolerance of 10 ppm, fragment mass tolerance of 0.2 Da and a maximum number of 2 missed cleavages. Fixed modifications included carbamidomethylation of cysteine, TMT 6-plex modification of lysine and peptide N-termini and variable modifications included oxidation of methionine and deamidation of asparagine or glutamine. Reporter version 0.2.13 (http://compomics.github.io/projects/reporter.html) was used for quantification of isobaric tags. Proteins were annotated for Reactome and KEGG pathway identifiers as well as gene ontology (GO) terms for biological processes (BP), molecular functions (MF) and, cellular components (CC). Results were analysed using Perseus version 1.5.3.1 (Max Planck Institute of Biochemistry) and included only proteins identified using a minimum of two unique peptides in addition to being present in all corresponding replicate sets with a 100% identification confidence. Average protein ratios were expressed relative to monolayer controls. K-mean pre-processing and average linkages

were used for hierarchical clustering. Multi-sample testing using log2(x) transformed relative abundance ratios, was conducted using ANOVA with a permutation-based false discovery rate (FDR) for truncation and an FDR of 0.01 with 250 randomizations. Volcano plots were generated using two-tailed t-tests with stringency of analysis controlled by an FDR of 0.01 with 250 randomizations and mean weighting. Principal component analysis (PCA) was done using a Benjamini-Hochberg cut-off method with a 0.01 FDR.

3. Results

3.1 Preliminary cytotoxicity in HepG2 monolayers

Known hepatotoxins, Ketoconazole and Troglitazone, were found to have high micromolar IC_{50} values (Figure 1) while Bromfenac mimicked the dose-response observed for the non-hepatotoxic Diphenhydramine and did not induce a dose-response at any of the concentrations investigated.

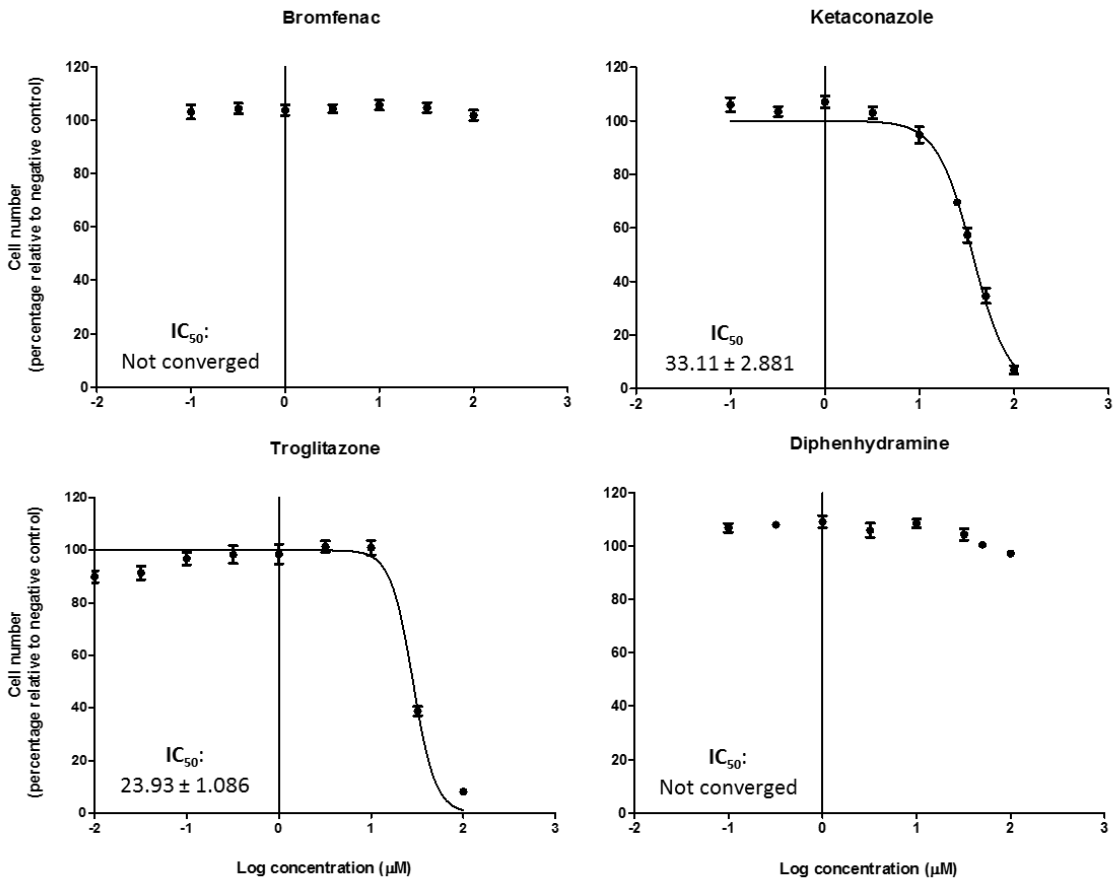

Figure 1: Dose-response curves and associated IC_{50} values (µM ± SEM) for Bromfenac, Ketoconazole, Troglitazone and Diphenhydramine obtained for HepG2 cells cultured as conventional monolayers and assayed using the SRB assay after 72 hours. *(2-column fitting)*

ROS, MMP, GSH and steatosis disrupt cellular homeostasis which can be associated with the initiation of cell death. Ketoconazole (Figure 2) and Troglitazone (Supplementary data II: Figure 1) induced similar concentration and time dependent changes in ROS, MMP, GSH and fatty acid accumulation. Decreased cell viability and MMP, with a consequent increase in caspase-3/7 activity, were observed simultaneously with decreased intracellular GSH and increased fatty acid accumulation. Diphenhydramine (Supplementary data II: Figure 2) and Bromfenac had no effect on HepG2 cell monolayers. For proteomic profiles, Ketoconazole and Troglitazone were used at their calculated IC_{20} of 20 µM and 15 µM respectively while Bromfenac and Diphenhydramine were used at their calculated C_{max} and 100x C_{max} of 25 µM and 30 µM respectively

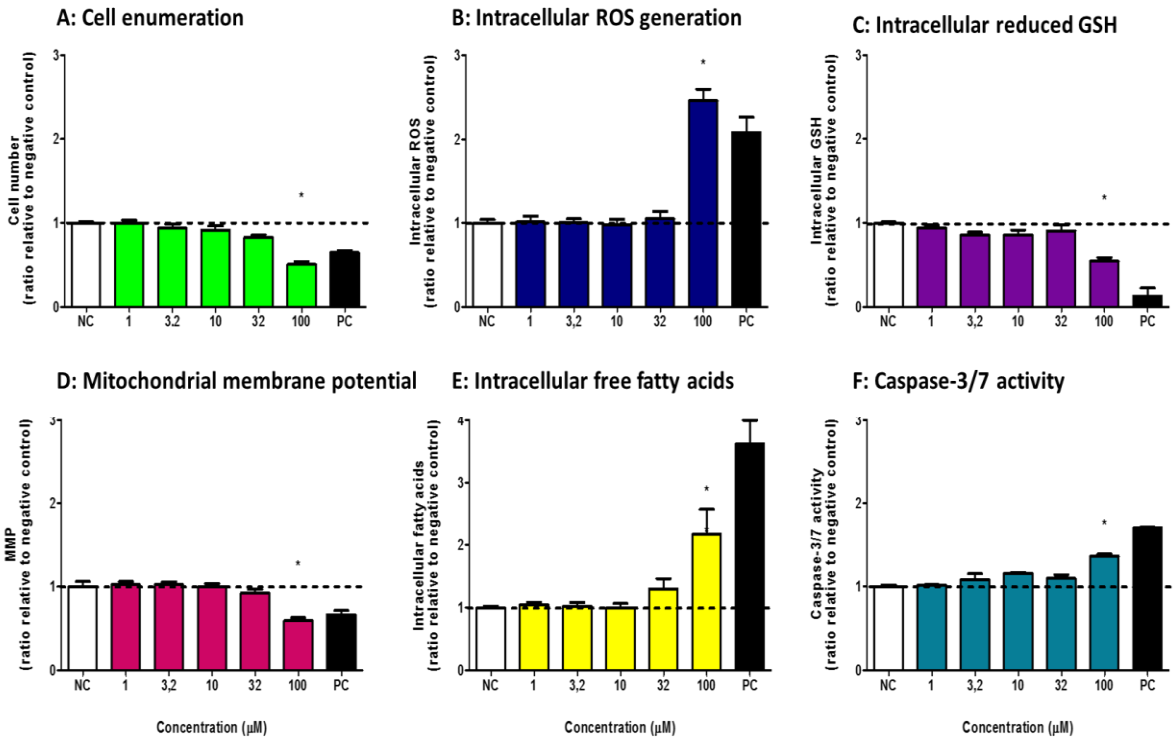

Figure 2: Bar graphs depicting the effect of Ketoconazole exposure for 24 hours on A) Cell enumeration, B) Intracellular ROS generation, C) Intracellular reduced GSH, D) MMP, E) Steatosis and F) Caspase-3/7 activity. NC: negative control, PC: positive control. Positive controls, provided in Supplementary II: Table 2, were statistically significantly reduced or increased as required for each assay. Significance (*) compared to the NC was defined as $p < 0.05$. *(2-column fitting, landscapre orientation)*

3.2 HepG2 monolayers and HepG2 3D spheroids

Monolayer cultures of HepG2 cells (Figure 3A) and size controlled, scaffold free, viable 3D spheroids were cultured (Figure 3B-C) for 4 days prior to drug exposure. Samples were compared using SDS-PAGE prior to stable isotope labelled mass spectrometry. Gel protein profiles demonstrated no obvious band differences between monolayer cultures exposed to drugs. However, spheroids exposed to Ketoconazole and Troglitazone at their respective IC_{20} demonstrated transient band alterations across various mass ranges (Figure 3D-E).

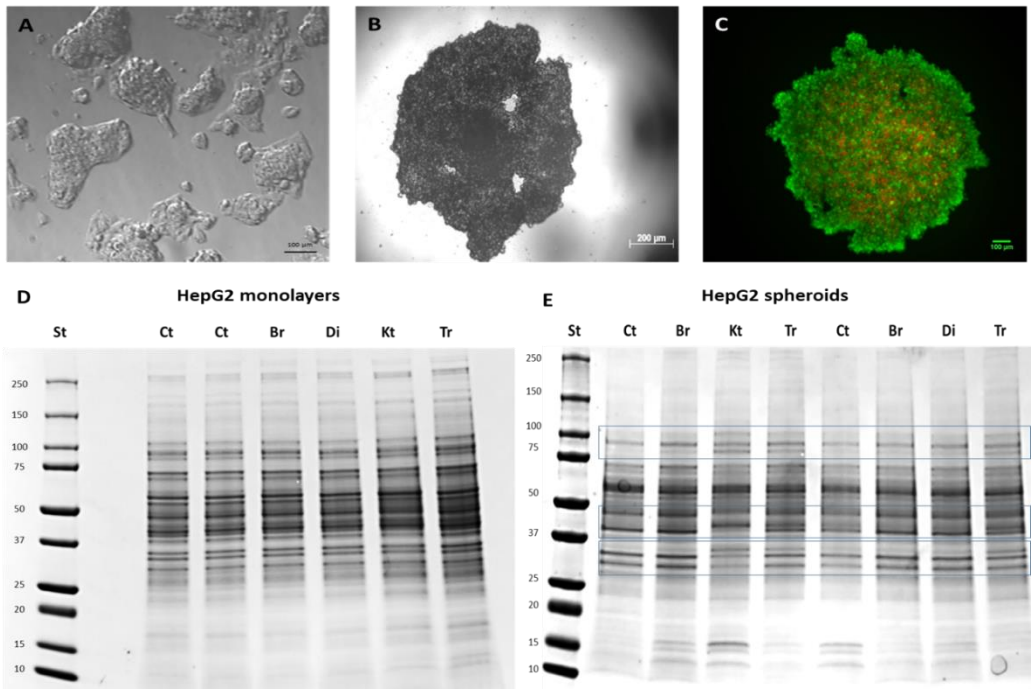

Figure 3: *A) HepG2 monolayer cultures (scale bar: 100 µm), B) HepG2 3D spheroid maintained in a hanging drop (scale bar: 200 µm), C) HepG2 3D control spheroid with FDA staining illustrating cell viability and non-specific PI staining (scale bar: 100 µm), D) Coomassie stained gel of HepG2 monolayers following drug exposure and E) Coomassie stained gel of HepG2 3D spheroids following drug exposure with band alterations highlighted across various mass ranges (25-37 kDa, 37-50 kDa and 75-100 kDa). St: Molecular mass standard, Ct: Control, Br: Bromfenac, Kt: Ketoconazole, Tr: Troglitazone.* (2-column fitting)

3.2.1 Proteome of HepG2 monolayers versus HepG2 3D spheroids

Identification and quantification of proteins for monolayer and 3D spheroids following exposure to Bromfenac or Troglitazone (CBT replicate sets) was 4701, 5030 and 4932 for replicates 1 to 3 respectively (Supplementary data I: CBT replicate 1, 2 and 3 default reports). The dataset was reduced to 3760 common proteins after applying the appropriate constraints (Supplementary data I: CBT replicates 1-3 proteins).

Similarly for Diphenhydramine and Ketoconazole (CDK replicate sets), replicates 1 to 3 had 5055, 4971 and 4680 proteins respectively (Supplementary data I: CDK replicate 1, 2 and 3 default reports) which was reduced to 3727 common proteins after applying the appropriate constraints (Supplementary data I: CDK replicates 1-3 proteins). Combining quantification of the HepG2 monolayer and 3D spheroid controls across all six experiments, provided a cohort of 3421 common proteins (Figure 4A and Supplementary data I: Average abundance 2D versus 3D) where hierarchical clustering grouped all monolayer culture replicates together. Although the 3D spheroids predominantly segregated away from monolayer cultures, some biological replicates correlated more closely with the HepG2 monolayers. This suggests a dynamic continuum of proteome changes which was not identical in each replicate experiment. Despite this variability, volcano plots (Figure 4B) identified 1163 proteins that met statistical cut-offs that clearly distinguish 2D versus 3D spheroid cultures. Of these 590 proteins were increased in abundance in 3D spheroids versus 573 which were reduced in abundance (Supplementary data I: Volcano plot 2Dv3D). Extreme outliers in these volcano plots were annotated (Supplementary data I: 2Dv3D). Abundance, 3D spheroids, of α-fetoprotein, α-2-HS-glycoprotein, Vitronectin and Fibulin-1 in this protein cohort were particularly noteworthy as these play a role in hepatic phenotypes and molecular organization of ECM architecture.

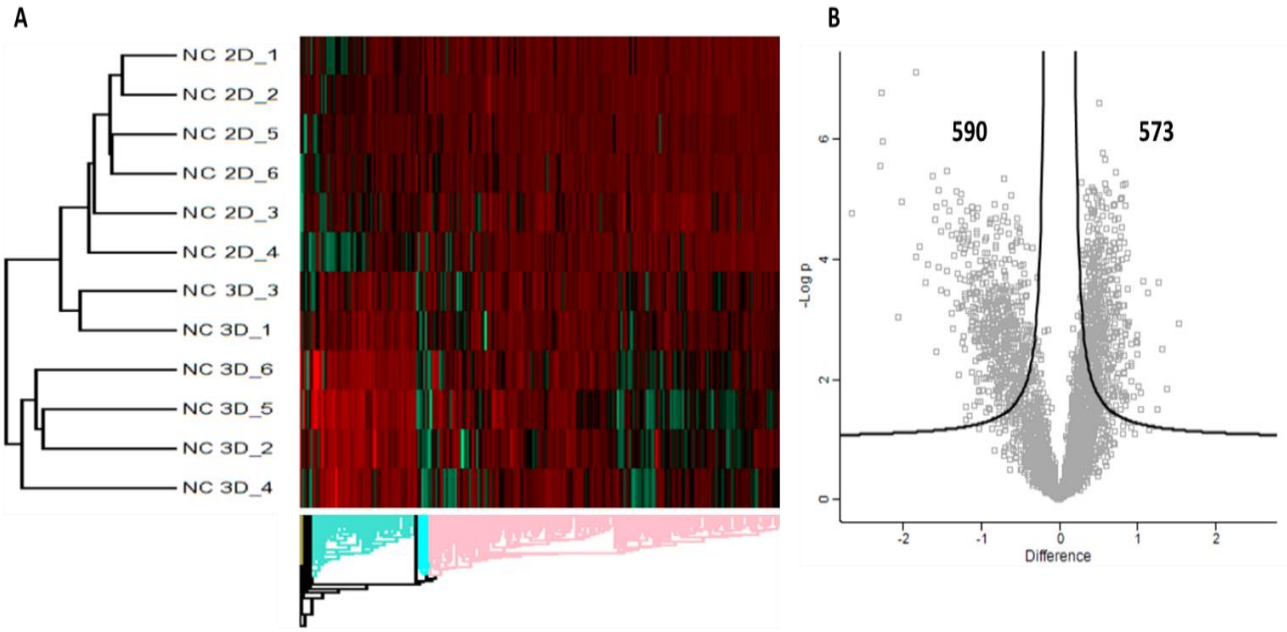

Figure 4: A) Hierarchical clustering of HepG2 cell monolayers (NC 2D) and spheroids (NC 3D) across six independent TMT replicate sets and B) Volcano plot comparing relative protein abundance in HepG2 cell monolayers versus 3D spheroids using an FDR of 0.01. (2-column fitting)

Principal component analysis clustered monolayer cultures distinctly in Component 1 (48.53%) and Component 2 (12.0%) of principal component space (Figure 5A). And while, 3D spheroids of HepG2 cells were spatially resolved from monolayers there was no ordered or predictable clustering across the 3D culture replicates. The localisation across principal component space again illustrated the variance observed in the hierarchical clustering analysis and could highlight the heterogeneity with which the HepG2 3D spheroids undergo proteomic transitions. While there is a possibility that technical features of mass-spectrometry acquisitions across replicates could result in some disparities, the tight clustering of six monoculture replicates suggests that proteomic differences are induced during the time course of spheroid culture.

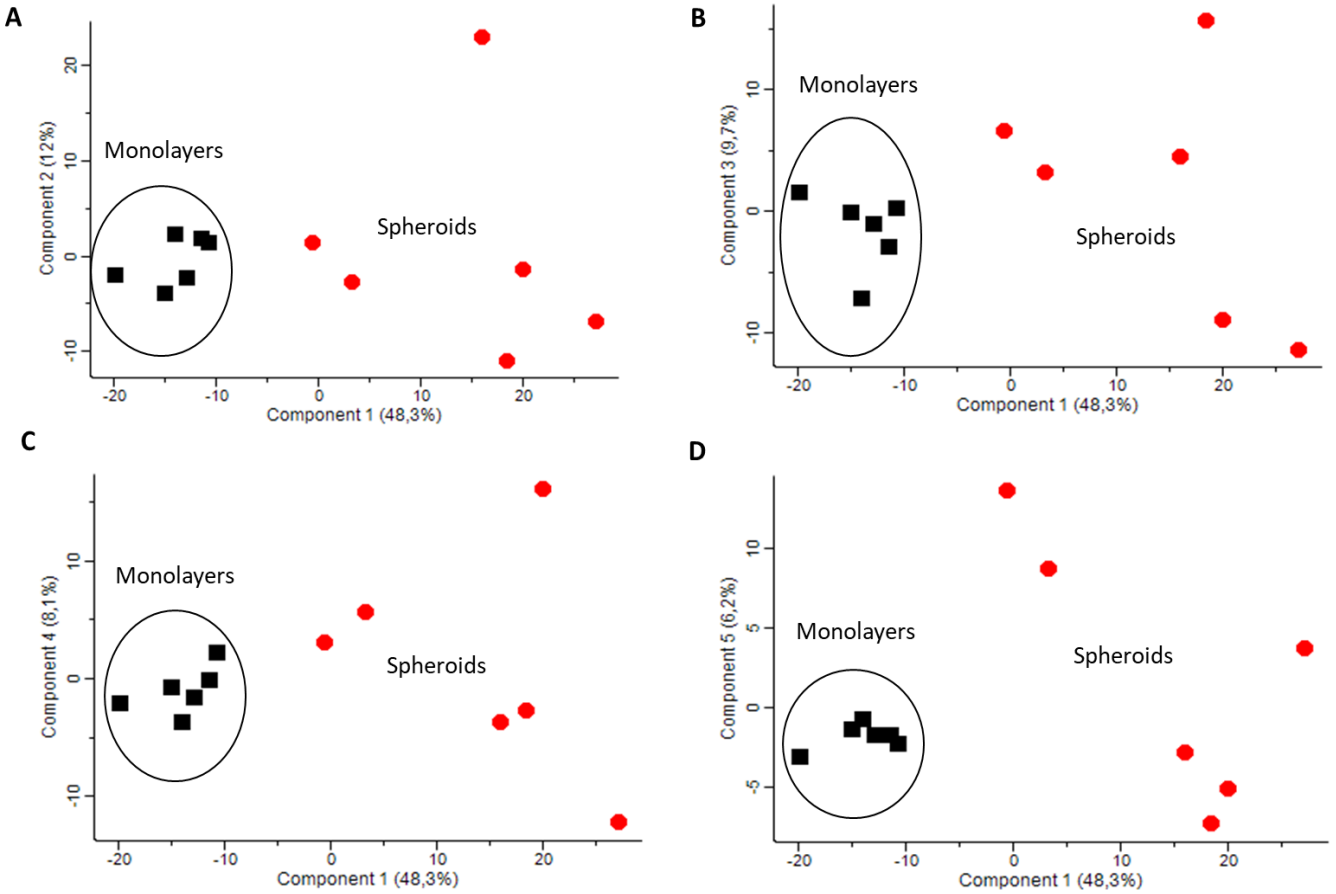

Figure 5: Principal component analysis of HepG2 cell monolayers (black squares, n=6) and 3D spheroids (red circles, n=6) comparing A) Component 1 versus Component 2, B) Component 1 versus Component 3, C) Component 1 versus Component 4 and D) Component 1 versus Component 5. *(2-column fitting)*

Potential modulation of the HepG2 phenotype was investigated by comparing the relative abundance of typical hepatic functional marker proteins. This found alpha-fetoprotein, apolipoprotein A-I, apolipoprotein A-II, serum albumin and alpha-2-HS-glycoprotein to be increased in 3D spheroids compared to monolayer cultures (Table 1, extracted from Supplementary data I: Average abundance, 2D versus 3D). Important plasma proteins predominantly synthesized by hepatocytes including alpha-2-HS-glycoprotein and albumin were increased 3-fold in hepatocytes from 3D spheroid cultures. Other hepatic markers and key regulators such as alpha-1-antitrypsin and hepatocyte nuclear factor 4-alpha (HNF4α) were similarly abundant. Phase I metabolizing proteins were not reliably identified in HepG2 cells with only three CYP450 proteins (CYP20A1,CYP2S1, CYP2W1) being consistent across replicates. Similar representation of the proteins cohort of phase II

metabolising enzymes and membrane transporters was observed suggesting that without targeted analysis from various cellular compartments, these essential proteins are not detected due to their limited abundance and lipophilic membrane association.

Spheroid cultures considerably alter cellular morphology compared to monolayer counterparts, which modifies cytoskeletal arrangement and ECM interactions Some ECM proteins, secreted by liver cell subpopulations were investigated for their contribution to differences observed between cultures. These proteins were not definitively altered in favour of one culture with tropomyosins, filamins, profilins, cofilins, destrin, some kinesins and catenins being similarly abundant. Whereas type I and II keratins, tubulins, integrins, fibronectin, vitronectin and laminins were increased in abundance in the 3D spheroid cultures. These data can be further interrogated for relationships governing morphological changes induced by hanging-drop cultures.

Table 1: Relative abundance, expressed relative to HepG2 monolayers, of hepatic markers, ADME proteins and cytoskeletal markers

Protein description	Accession	Monolayer Mean ± SD	Spheroids Mean ± SD	-LOG(P-value)
Hepatic markers				
Alpha-1-antitrypsin	P01009	1.00 ± 0.11	0.88 ± 0.10	N/A
Alpha-2-HS-glycoprotein	P02765	1.00 ± 0.08	3.11 ± 0.28	5.38
Alpha-fetoprotein	P02771	1.00 ± 0.07	4.99 ± 0.640	5.97
Amine oxidase [flavin-containing] A	P21397	1.00 ± 0.04	1.67 ± 0.13	3.50
Amine oxidase [flavin-containing] B	P27338	1.00 ± 0.08	2.06 ± 0.23	3.17
Apolipoprotein A-I	P02647	1.00 ± 0.07	2.18 ± 0.14	4.87
Apolipoprotein A-II	P02652	1.00 ± 0.14	2.53 ± 0.30	2.85
Apolipoprotein B-100	P04114	1.00 ± 0.03	1. 30 ± 0.09	N/A
Hepatocyte nuclear factor 4-alpha	P41235	1.00 ± 0.08	1.05 ± 0.19	N/A
Serum albumin	P02768	1.00 ± 0.06	3.16 ± 0.45	4.65
ADME proteins: Phase I				
Cytochrome P450 20A1	Q6UW02	1.00 ± 0.04	1.51 ± 0.19	N/A
Cytochrome P450 2S1	Q96SQ9	1.00 ± 0.06	1.14 ± 0.10	N/A
Cytochrome P450 2W1	Q8TAV3	1.00 ± 0.02	1.28 ± 0.04	4.18
ADME proteins: Phase II				
UDP-glucuronosyltransferase 2A3	Q6UWM9	1.00 ± 0.05	2.41 ± 0.22	5.08
Glutathione reductase, mitochondrial	P00390	1.00 ± 0.07	0.940± 0.09	N/A
Glutathione S-transferase kappa 1	Q9Y2Q3	1.00 ± 0.03	0.85 ± 0.04	N/A
Glutathione S-transferase Mu 3	P21266	1.00 ± 0.02	0.89 ± 0.13	N/A

Glutathione S-transferase omega-1	P78417	1.00 ± 0.06	0.64 ± 0.05	2.65
Glutathione S-transferase theta-1	P30711	1.00 ± 0.07	0.64 ± 0.07	2.35
Glutathione synthetase	P48637	1.00 ± 0.03	0.76 ± 0.04	3.00
ADME proteins: Phase III				
Multidrug resistance protein 1	P08183	1.00 ± 0.07	1.06 ± 0.09	N/A
Multidrug resistance-associated protein 1	P33527	1.00 ± 0.04	1.44 ± 0.09	2.97
Multidrug resistance-associated protein 4	O15439	1.00 ± 0.21	2.47 ± 0.53	1.50
Cytoskeletal arrangement				
Keratin, type I cytoskeletal 10	P13645	1.00 ± 0.06	2.85 ± 0.28	4.94
Keratin, type I cytoskeletal 18	P05783	1.00 ± 0.03	1.37 ± 0.18	N/A
Keratin, type I cytoskeletal 9	P35527	1.00 ± 0.07	2.68 ± 0.27	4.80
Keratin, type II cytoskeletal 1	P04264	1.00 ± 0.07	2.73 ± 0.21	5.48
Keratin, type II cytoskeletal 5	P13647	1.00 ± 0.09	2.62 ± 0.24	4.39
Keratin, type II cytoskeletal 6B	P04259	1.00 ± 0.07	2.51 ± 0.21	5.13
Keratin, type II cytoskeletal 8	P05787	1.00 ± 0.04	1.42 ± 0.18	N/A
Tubulin alpha-1B chain	P68363	1.00 ± 0.03	1.00 ± 0.05	N/A
Tubulin alpha-1C chain	Q9BQE3	1.00 ± 0.03	1.00 ± 0.05	N/A
Tubulin beta chain	P07437	1.00 ± 0.02	0.92 ± 0.05	N/A
Tubulin beta-3 chain	Q13509	1.00 ± 0.02	0.91 ± 0.05	N/A
Tubulin beta-4B chain	P68371	1.00 ± 0.02	0.92 ± 0.05	N/A
Tubulin gamma-1 chain	P23258	1.00 ± 0.04	1.23 ± 0.08	N/A

3.3 Proteomic profiling of hepatotoxicity

Within each triplicate set of drug exposed monolayers and 3D spheroids, hierarchical clustering generally co-segregated monolayers and 3D spheroids regardless of the presence or absence of drugs. This is illustrated with Bromfenac exposed samples (Figure 6A) where twelve TMT labelled samples formed major branches distinguishing monolayers and 3D spheroids. Exposure of the cultures to Bromfenac in both monolayer (Figure 6B) or 3D spheroid cultures (Figure 6C) did not show any changes in protein abundances that met statistical thresholds when compared to respective controls. When performing hierarchical clustering on averaged replicates, the majority again bifurcated clearly into monolayers and 3D spheroids (Figures 6E, 6F and 6G) with the exception of Troglitazone (Figure 6F) in which samples were subdivided within the spheroid negative control as the major node.

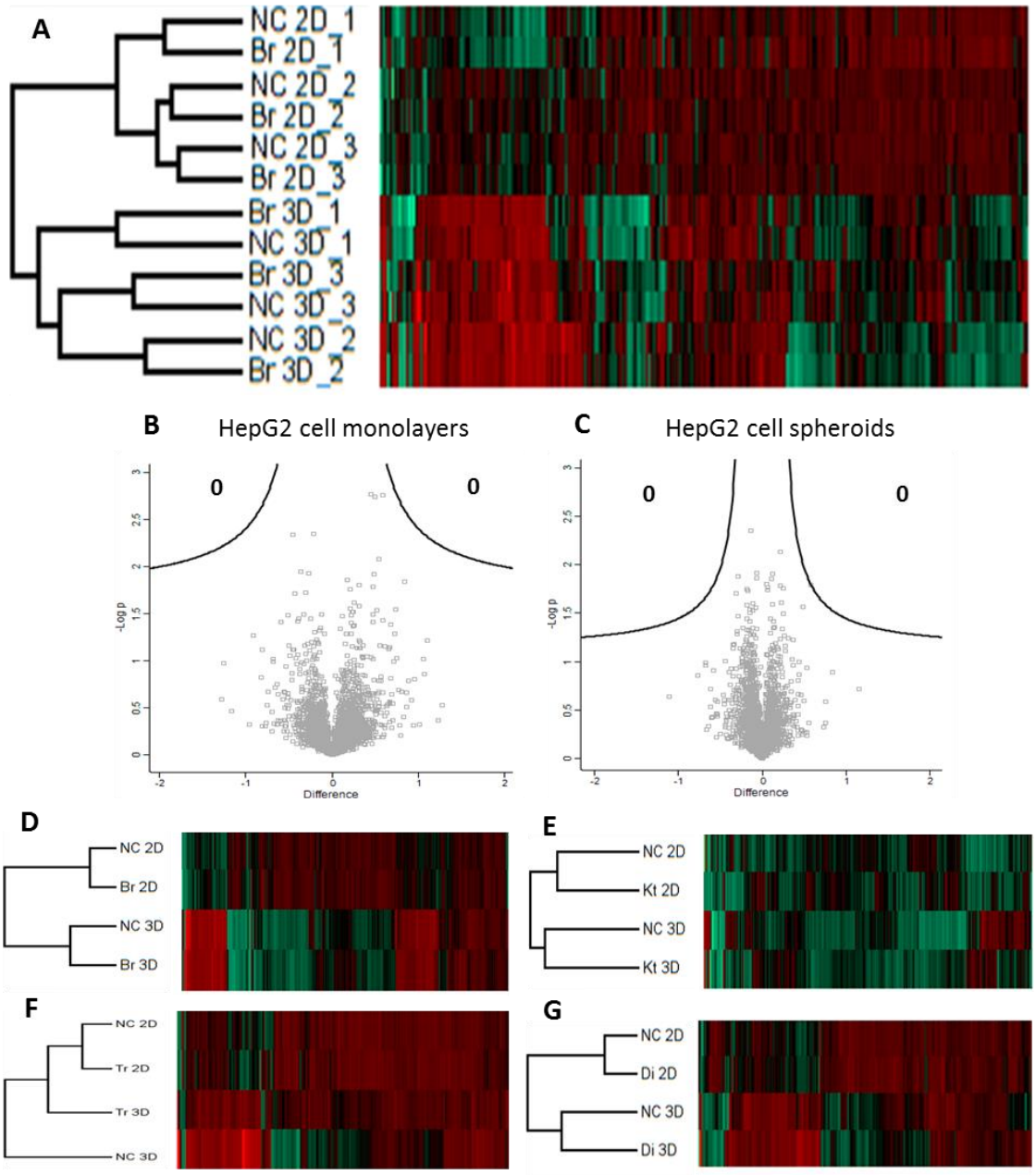

Figure 6: A) Hierarchical clustering of individual replicates of HepG2 cell monolayers (NC 2D) and 3D spheroids (NC 3D) exposed to Bromfenac (Br), B) Volcano plot comparing HepG2 cell monolayers exposed to Bromfenac, C) Volcano plot comparing HepG2 cell 3D spheroids exposed to Bromfenac, D) Hierarchical clustering of combined replicates exposed to Bromfenac, E) Hierarchical clustering of combined replicates exposed to Ketaconazole (Kt), F) Hierarchical clustering of combined replicates exposed to Troglitazone (Tr), and G) Hierarchical clustering of combined replicates exposed to non-hepatotoxic Diphenhydramine (Di). *(2-column fitting, landscape orientation)*

Principal component analysis for the Bromfenac and Troglitazone exposed cultures (Figure 7) also clustered monolayer cultures together in Component 1 (53.4%) versus Component 2 (14.6%) or Component 3 (10.7%). Monolayers were again distinctly separate from 3D spheroids which had no uniform distribution. This suggests large heterogeneity in the maturation of spheroid cultures resulting in distinct sub-populations of spheroids phenotypes which dominate over potential abundance changes in proteins induced by each drug. Despite this unpredictable clustering of spheroids, postulated to relate to the formation of multiple hepatic proteomes, PCA spatially resolved the culturing techniques and reiterated the absence of a distinct proteomic profile following exposure to repeated exposure to low concentrations of hepatotoxic drugs.

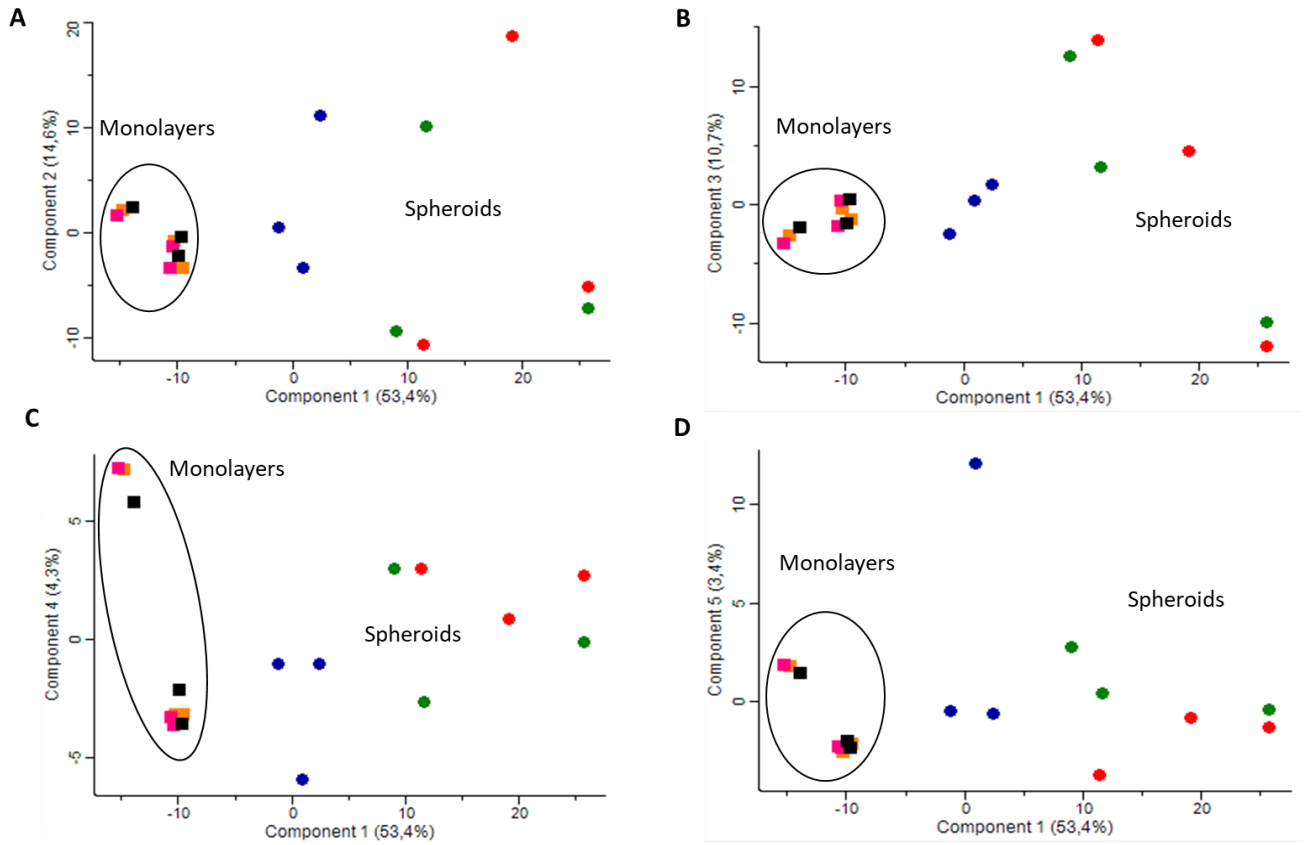

Figure 7: Principal component analysis of controls, Bromfenac and Troglitazone exposed (n=3) HepG2 monolayers and 3D spheroids. A) Component 1 versus Component 2, B) Component 1 versus Component 3, C) Component 1 versus Component 4, and D) Component 1 versus Component 5. Negative control monolayers: black square; Negative control spheroids: red circle; Bromfenac monolayers: orange square; Bromfenac spheroids: green circle; Troglitazone monolayers: pink square and Troglitazone spheroids: blue circle. *(2-column fitting)*

4. Discussion

HepG2 cells cultured as 3D spheroids reportedly exhibit altered gene expression of albumin, urea, xenobiotic transcription factors, phase I and II drug metabolizing enzymes and transporters (Ramaiahgari *et al.*, 2014). However, proteomic differences between human adult hepatocytes and HepG2 cells have been delineated, with the value of HepG2 cells in pharmacological and toxicokinetic analysis continuing to be questioned (Wiśniewski *et al.*, 2016). Physiological features dictating a cellular phenotype are derived from whether cells are in a continuous exponential growth phase or in a state of dynamic equilibrium. Transitions between phases can be spontaneous with HepG2/C3A cells cultured as spheroids considered more phenotypically enabled to execute advanced

physiological functions (Wrzesinski *et al.*, 2014). However, the reproducibility of these transitions of immortalized cell lines is influenced by the cellar origin, culture format and consistency in expression of drug-metabolising enzyme during passaging.

Wrzesinski *et al*. postulated that following trypsinization, physiological functions of HepG2/C3 cells in monolayers are focussed on repair and proliferation while spheroids can re-differentiate and mature overtime (Wrzesinski *et al.*, 2013). This could describe why culturing HepG2 cells as 3D spheroids augmented expression of approximately 34% of the quantified proteins (1163 of 3241) and why these changes were not overwhelmingly linked to specific cellular functions. These altered proteins could be correlated to and be dependent on the type of spheroid culture technique and the status of differentiation prior to forming spheroids.

Spheroids formed using proliferating cells generally consist of an outer proliferation zone, intermediate quiescent zone with the potential of developing an inner necrotic core occurring if certain dimensions are exceeded. (Mehta *et al.*, 2012). Spheroid zones, each with a distinct proteome, could form inconsistently across spheroids resulting in variable protein abundances across biological replicates as observed in PCA plots. This suggests replicates are averaging multiple versions of the HepG2 proteome with each spheroid potentially containing various numbers of cells in the exponential, equilibrium or quiescent phases. Phenotypic reproducibility is considered a major advantage of immortalized cell lines, here this well demonstrated in monocultures but this notion is challenged when HepG2 cells are cultured as spheroids under the conditions described. However, it is evident that 3D cultures of HepG2 cells are distinguishable from monolayers but that the continuum of changes needs to be better investigated.

HepG2 cell spheroids have reduced proliferation, are capable of self-organization and differentiation. Despite altered gene expression of albumin, urea, xenobiotic transcription factors, metabolizing enzymes and transporters being apparent, pronounced proteomic differences still exist when compared to PHHs (Hurrell, Segeritz*, et al.*, 2018; Ramaiahgari *et al.*, 2014). ADME associated

proteins, are essential for metabolic competence and include over 320 proteins from more than 50 protein families which are mostly found in low abundance, integral membrane proteins (Sun *et al.*, 2002; Vildhede *et al.*, 2015). Here, metabolizing enzymes were poorly identified and did not contribute significantly to the protein abundance differences observed. While unable to salvage metabolic competence in 3D spheroids, these HepG2 cell cultures highlighted essential features associated with the plasticity of immortalized cell lines and the variability in proteomic changes. As a result the ability to observe meaningful signatures of hepatotoxicity was challenging as the hepatotoxins selected are not as potent as their corresponding metabolites and some proteins, although changing significantly, may have been completely overwhelmed by changes in abundant proteins.

Bromfenac has five reactive metabolites including a cyclic amide and two pairs of polar diastereoisomeric glucuronide metabolites (Walgren *et al.*, 2005). Despite no *in vitro* toxicity being observed here or in other studies (Otto *et al.*, 2008), it was considered advantageous to include this drug in the panel to have a non-hepatotoxic drug (Diphenhydramine), a hepatotoxic non-responder (Bromfenac) and hepatotoxic drugs inducing dose-responses (Ketaconazole and Troglitazone) to provide scope to the proteomic analysis. Although the difference between monolayers and 3D spheroids overwhelmed the hierarchical clustering and PCA the bioactivation of Ketaconazole and Troglitazone differ and therefore proteins involved in these pathways were investigated.

Ketoconazole undergoes N-deacetylation to form N-deacetyl-ketoconazole (DAK) after which a series of flavin-containing monooxygenase (FMO) dependent reactions result in N-hydroxy DAK which finally forms a reactive dialdehyde (Walgren *et al.*, 2005). Human FMO enzymes, FMO1 and FMO3, have long been implicated in catalysing N-hydroxylation of DAK, with arylacetamide deacetylase (AADAC) confirmed as the primary enzyme responsible for Ketoconazole hydrolysis to DAK (Fukami

et al., 2016). AADAC was not identified in the data collected in this study, and neither were the most applicable FMO enzymes required for further catalysis.

Troglitazone is composed of a thiazolidinedione ring common to the class of glitazone drugs, and a unique chromane ring which each undergo distinct oxidative bioactivation. The chromane ring undergoes oxidation via multiple non-specific P450 enzymes to a reactive o-quinone methide while the thiazolidinedione ring undergoes an oxidative cleavage via CYP3A4 to α-ketoisocyante via a sulfenic acid intermediates (Kassahun *et al.*, 2001; Walgren *et al.*, 2005). These data sets poorly quantified CYP enzymes (CYP20A1, CYP2S1, CYP2W1) which could be responsible for the limited ability to form sufficient bioactive metabolites integral to Troglitazone toxicity.

5. Conclusions

Culturing HepG2 cells as static 3D spheroids altered the cellular proteome as would be anticipated based on changes in cell-cell communication and ECM of 3D spheroids and the phenotypic plasticity of HepG2 cells. However, these changes were not reproducible across replicates while conventional monolayer cultures displayed greater phenotypic stability. Despite this, increased abundance of proteins indicative of a more mature hepatic phenotype were evident in 3D spheroids. These data sets suggest that differences in exponential, equilibrium or quiescent phases or zones of 3D spheroids could be responsible for the proteomic heterogeneity. In a pilot study of drug exposure to known hepatotoxins, these proteomic changes did not identify meaningfully altered proteins groups that can be definitively associated with a toxic response as a result of a still limited capacity to form reactive metabolites. Here, insight into the dynamics of HepG2 cells in 3D spheroids and extensive, in-depth quantification of these changes is provided. It is hypothesised that a prolonged incubation time for 3D spheroid cultures could reduce the heterogeneity observed in the proteome and reconcile the differences in the proteome providing a more a reproducible phenotype for applications which warrant the use of HepG2 cells.

Author's contribution and conflict of interest

TH and ADC designed and planned the experiments. TH performed the cell culture, protein sample preparation, isobaric tagging and data analysis. All authors contributed to the data interpretation and to the writing of the manuscript. None of the authors have any competing interests to declare.

Acknowledgements

The authors would like to acknowledge Dr M Vlok from the Central Analytical Facility at the University of Stellenbosch for performing the LC-MS/MS analysis and to Mr AA Ellero for providing the 3D spheroid fluorescence images.

Funding

This work was supported by the National Research Foundation of South Africa (NRF) Thuthuka PhD funding track grant (No. 87880). Any opinion, findings, conclusions or recommendation expressed in this material is that of the author(s) and not that of the NRF. In addition, TH was supported by a UK Commonwealth Split-site Scholarship (ZACS-2014-653) and a Commonwealth, European and International Cambridge Trust Scholarship (USN: 302989247; App No: 10326363).

References

Ahuja V. and Sharma S. (2014). Drug safety testing paradigm, current progress and future challenges: An overview. *J. Appl. Toxicol.* **34**(6), 576-594.

Bell C. C.*, et al.* (2016). Characterization of primary human hepatocyte spheroids as a model system for drug-induced liver injury, liver function and disease. *Sci. Rep.* **6**, 25187.

Bhakuni G. S.*, et al.* (2016). Animal models of hepatotoxicity. *Inflamm. Res.* **65**(1), 13-24.

Blyden G. T.*, et al.* (1986). Pharmacokinetics of diphenhydramine and a demethylated metabolite following intravenous and oral administration. *J. Clin. Pharmacol.* **26**(7), 529-533.

Cai J.*, et al.* (2012). Protocol for directed differentiation of human pluripotent stem cells toward a hepatocyte fate. *StemBook*.

Chen M.*, et al.* (2011). FDA-approved drug labeling for the study of drug-induced liver injury. *Drug Discov Today* **16**(15), 697-703.

Duret C.*, et al.* (2007). Isolation, characterization, and differentiation to hepatocyte-like cells of nonparenchymal epithelial cells from adult human liver. *Stem Cells* **25**(7), 1779-1790.

Feng Y.*, et al.* (2014). Global analysis of protein structural changes in complex proteomes. *Nat. Biotechnol.* **32**(10), 1036-1044.

Foty R. (2011). A simple hanging drop cell culture protocol for generation of 3D spheroids. *JoVE* (51), 2720.

Fukami T.*, et al.* (2016). Human arylacetamide deacetylase hydrolyzes ketoconazole to trigger hepatocellular toxicity. *Biochem. Pharmacol.* **116**, 153-161.

Gale E. A. (2006). Troglitazone: The lesson that nobody learned? *Diabetologia* **49**, 1–6.

Gelotte C. K.*, et al.* (2018). Single-dose pharmacokinetic study of diphenhydramine HCL in children and adolescents. *Clin. Pharmacol. in Drug Devel.* **7**(4), 400-407.

Griffith L. G. and Swartz M. A. (2006). Capturing complex 3D tissue physiology in vitro. *Nat. Rev. Mol Cell Bil.o* **7**(3), 211-224.

Heidariyan Z.*, et al.* (2018). Efficient and cost-effective generation of hepatocyte-like cells through microparticle-mediated delivery of growth factors in a 3D culture of human pluripotent stem cells. *Biomaterials* **159**, 174-188.

Högger P. and Rohdewald P. (1993). Pharmacokinetics of bromfenac in healthy subjects after single oral administration of three different doses. *Arzneimittelforschung* **43**(10), 1114-1118.

Hughes B. (2008). Industry concern over EU hepatotoxicity guidance. *Nature Reviews Drug Discovery* **7**, 719.

Hunter E. B.*, et al.* (1999). Bromfenac (duract)-associated hepatic failure requiring liver transplantation. *Am J Gastroenterol.* **94**(8), 2299-2301.

Hurrell T.*, et al.* (2018). Characterization and reproducibility of HepG2 hanging drop spheroids toxicology in vitro. *Toxicol. In Vitro* **50**, 86-94.

Hurrell T.*, et al.* (2018). Proteomic comparison of various hepatic cell cultures for preclinical safety pharmacology. *Toxicol. Sci.*, **164**(1): 229–239.

Kaku K.*, et al.* (2015). Efficacy and safety of fasiglifam (tak-875), a G-protein-coupled receptor 40 agonist, in japanese patients with type 2 diabetes inadequately controlled by diet and exercise: A randomized, double-blind, placebo-controlled, phase III trial. *Diabetes Obes. Metab.* **17**(7), 675-681.

Kamei K.*, et al.* (2017). Robust direct differentiation and maturation of human pluripotent stem cells to hepatocyte-like cells. *bioRxiv*, 232215.

Kassahun K.*, et al.* (2001). Studies on the metabolism of troglitazone to reactive intermediates *in vitro* and *in vivo*. Evidence for novel biotransformation pathways involving quinone methide formation and thiazolidinedione ring scission. *Chem. Res. Toxicol.* **14**(1), 62-70.

Kinter L. B. and Valentin J. P. (2002). Safety pharmacology and risk assessment. *Fundam. Clin. Pharmacol.* **16**(3), 175-182.

Kline N. S. (1970). Monoamine oxidase inhibitors: An unfinished picaresque tale. *Discov. Biol. Psychiatry* **194**.

Klingelhutz A. J.*, et al.* (2018). Scaffold-free generation of uniform adipose spheroids for metabolism research and drug discovery. *Sci. Rep.* **8**(1), 523.

Kola I. and Landis J. (2004). Can the pharmaceutical industry reduce attrition rates? *Nat Rev Drug Discov.* **3**(8), 711-716.

Koyama S.*, et al.* (2018). Evaluation of the metabolic capability of primary human hepatocytes in three-dimensional cultures on microstructural plates. *Biopharm. Drug Disposition* **39**(4), 187-195.

Krewski D.*, et al.* (2009). Toxicity testing in the 21st century: Implications for human health risk assessment. *Risk Anal.* **29**(4), 474-479.

Lauschke V. M.*, et al.* (2016). Novel 3D culture systems for studies of human liver function and assessments of the hepatotoxicity of drugs and drug candidates. *Chem. Res. Toxicol.* **29**(12), 1936-1955.

Mehta G.*, et al.* (2012). Opportunities and challenges for use of tumor spheroids as models to test drug delivery and efficacy. *J. Control. Release* **164**(2), 192-204.

Miyamoto D.*, et al.* (2018). Changes in HepG2 spheroid behavior induced by differences in the gap distance between spheroids in a micropatterned culture system. *J Biosci Bioeng* **125**(6), 729-735.

Mueller D.*, et al.* (2014). 3D organotypic HepaRG cultures as *in vitro* model for acute and repeated dose toxicity studies. *Toxicol. In Vitro* **28**(1), 104-112.

Niles A. L.*, et al.* (2009). *In vitro* viability and cytotoxicity testing and same-well multi-parametric combinations for high throughput screening. *Curr.. Chem Genom.* **3**, 33-41.

Otto M.*, et al.* (2008). Development of an in vitro assay for the investigation of metabolism-induced drug hepatotoxicity. *Cell Biol. Toxicol.* **24**(1), 87.

Paech F.*, et al.* (2018). Mechanisms of mitochondrial toxicity of the kinase inhibitors ponatinib, regorafenib and sorafenib in human hepatic HepG2 cells. *Toxicology* **395**, 34-44.

Panek M.*, et al.* (2018). The formation of intestinal organoids in a hanging drop culture. *Cytotechnology*, 1-11.

Ramaiahgari S. C.*, et al.* (2014). A 3D in vitro model of differentiated HepG2 cell spheroids with improved liver-like properties for repeated dose high-throughput toxicity studies. *Arch. Toxicol*. **88**(5), 1083-1095.

Ramirez T.*, et al.* (2018). Prediction of liver toxicity and mode of action using metabolomics in vitro in HepG2 cells. *Arch. Toxicol.* **92**(2), 893-906.

Rebelo S. P.*, et al.* (2017). Three-dimensional co-culture of human hepatocytes and mesenchymal stem cells: Improved functionality in long-term bioreactor cultures. *J. Tissue Eng. Regen. Med.* **11**(7), 2034-2045.

Redfern W. S.*, et al.* (2002). Safety pharmacology – a progressive approach. *Fundam. Clin. Pharmacol.* **16**(3), 161-173.

Saito J.*, et al.* (2016). High content analysis assay for prediction of human hepatotoxicity in HepaRG and HepG2 cells. *Toxicol. In Vitro* **33**, 63-70.

Shah U.K.*, et al.* (2018). A three-dimensional *in vitro* HepG2 cells liver spheroid model for genotoxicity studies. *Muta. Res. Gene. Toxicol. Environ. Mutagen.* **825**, 51-58.

Sun L. Z.*, et al.* (2002). ADME-AP: A database of ADME associated proteins. *Bioinformatics* **18**(12), 1699-1700.

van Tonder J. J. (2011). Development of an *in vitro* mechanistic toxicity screening model using cultured hepatocytes. Doctoral Thesis, University of Pretoria.

Vichai V. and Kirtikara K. (2006). Sulforhodamine B colorimetric assay for cytotoxicity screening. *Nat. Protoc.* **1**(3), 1112-1116.

Vildhede A.*, et al.* (2015). Comparative proteomic analysis of human liver tissue and isolated hepatocytes with a focus on proteins determining drug exposure. *J. Proteome Res.* **14**(8), 3305-3314.

Walgren J. L.*, et al.* (2005). Role of metabolism in drug-induced idiosyncratic hepatotoxicity. *Crit. Rev. Toxicol.* **35**(4), 325-361.

Wiśniewski J. R.*, et al.* (2016). In-depth quantitative analysis and comparison of the human hepatocyte and hepatoma cell line HepG2 proteomes. *J. Proteomics* **136**, 234-247.

Wrzesinski K. and Fey S. J. (2013). After trypsinisation, 3D spheroids of A3A hepatocytes need 18 days to re-establish similar levels of key physiological functions to those seen in the liver. *Toxicol. Res.* **2**(2), 123-135.

Wrzesinski K.*, et al.* (2014). The cultural divide: Exponential growth in classical 2D and metabolic equilibrium in 3D environments. *PLoS One* **9**(9), 1-15.

Yang Y.*, et al.* (2018). Bavachin induces apoptosis through mitochondrial regulated er stress pathway in HepG2 cells. *Biol. Pharm. Bull.* **41**(2), 198-207.

Manuscript title:

Proteomic responses of HepG2 cell monolayers and 3D spheroids to selected hepatotoxins

Supplementary data II

Manuscript ID: TOXLET_2018_90

Submission date: 25/08/2018

Revision date: 28/09/2018

Authors and affiliations:

Tracey Hurrell[a,l] (tracey.hurrell@ki.se)

Kathryn S. Lilley[b] (k.s.lilley@bioc.cam.ac.uk)

Allan Duncan Cromarty[a] (duncan.cromarty@up.ac.za)

[a]Department of Pharmacology, Faculty of Health Sciences, School of Medicine,

University of Pretoria, Private Bag X323, Arcadia, 0007, South Africa

[b]Cambridge Centre for Proteomics, Department of Biochemistry,

University of Cambridge, Tennis Court Road, Cambridge CB2 1QR, United Kingdom

[l] Section of Pharmacogenetics, Department of Physiology and Pharmacology,

Karolinska Institutet, Solnavägen 9, 171 65 Solna, Sweden

Table 1: Study drugs with their associated therapeutic class, FDA listing and market status

Drug	Therapeutic class	FDA listing (Chen et al. 2011)	Market status (for oral administration)
Bromfenac	NSAID	Most DILI concern (2nd)	Withdrawn (1998)
Ketoconazole	Antifungal	Most DILI concern (9th)	Withdrawn (2013)
Troglitazone	Antidiabetic	Most DILI concern (7th)	Withdrawn (2000)
Diphenhydramine	Antihistamine	No DILI concern	On the market

Drugs were withdrawn for oral administration, Bromfenac has been remarketed for ophthalmic applications and various topical preparations of Ketoconazole are available

Table 2: Parameters measured using the multi-parametric assay model showing the dye, dye concentration, excitation-emmission wavelengths and positive controls

Parameter	Dye	Concentration	Excitation-emission (nm)	Positive control
CV	SRB	0.057% (m/v)	Absorbance	Rotenone (100 nM)
ROS	H_2-DCF-DA	10 µM	485 / 520	p-Chloranil (5 µM)
GSH	Monochlorobimane	16 µM	355 / 460	N-ethylmalemide (50 µM)
MMP	JC-1	10 µM	485 / 520 (green) 492 / 590 (red)	Rotenone (100 nM)
Steatosis	Nile red	1 µM	544 / 590	Oleic acid (200 µM)
Apoptosis	Ac-DEVD-AMC	4 µM	355 / 460	Rotenone (100 nM)

Table 3: Tandem mass tag labelling to compare HepG2 cells as monolayers and spheroids before and after exposure to Bromfenac and Troglitazone

TMT label	Replicate 1	Replicate 2	Replicate 3
126	Troglitazone spheroids	Troglitazone spheroids	Control monolayers
127	Bromfenac spheroids	Bromfenac spheroids	Bromfenac monolayers
128	Control spheroids	Control spheroids	Troglitazone monolayers
129	Troglitazone monolayers	Troglitazone monolayers	Control spheroids
130	Bromfenac monolayers	Bromfenac monolayers	Bromfenac spheroids
131	Control monolayers	Control monolayers	Troglitazone spheroids

Table 4: Tandem mass tag labelling to compare HepG2 cells as monolayers and spheroids before and after exposure to Diphenhydramine and Ketoconazole

TMT label	Replicate 1	Replicate 2	Replicate 3
126	Ketoconazole spheroids	Ketoconazole spheroids	Control monolayers
127	Diphenhydramine spheroids	Diphenhydramine spheroids	Diphenhydramine monolayers
128	Control spheroids	Control spheroids	Ketoconazole monolayers
129	Ketoconazole monolayers	Ketoconazole monolayers	Control spheroids
130	Diphenhydramine monolayers	Diphenhydramine monolayers	Diphenhydramine spheroids
131	Control monolayers	Control monolayers	Ketoconazole spheroids

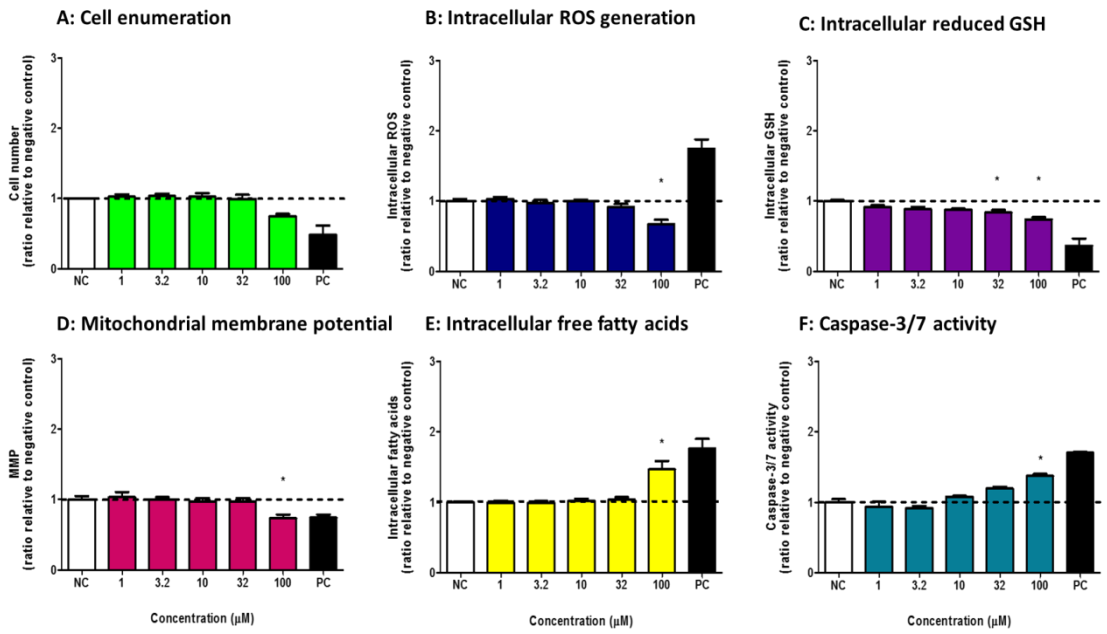

Figure 1: Bar graphs depicting the effect of Troglitazone exposure for 24 hours on A) Cell enumeration, B) Intracellular ROS generation, C) Intracellular reduced GSH, D) MMP, E) Steatosis and F) Caspase-3/7 activity. NC: negative control, PC: positive control. Each positive control was statistically significantly reduced or increased as required for each assay. Significance (*) compared to the NC was defined as $p < 0.05$.

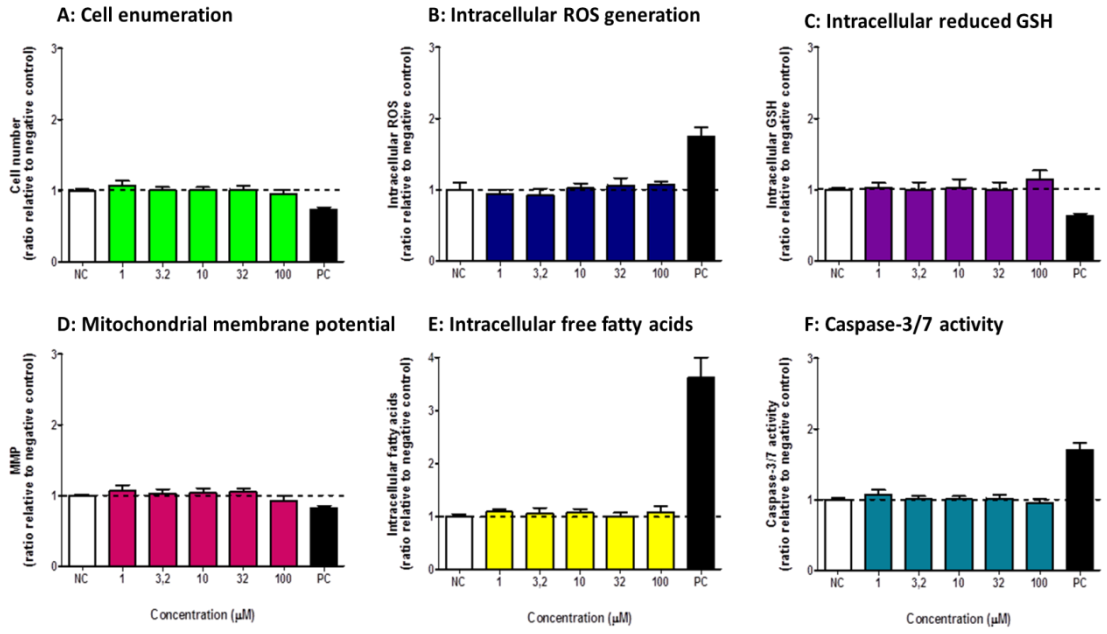

Figure 2: Bar graphs depicting the effect of Diphenhydramine exposure for 24 hours on A) Cell enumeration, B) Intracellular ROS generation, C) Intracellular reduced GSH, D) MMP, E) Steatosis and F) Caspase-3/7 activity. NC: negative control, PC: positive control. Each positive control was statistically significantly reduced or increased as required for each assay. Significance (*) compared to the NC was defined as $p < 0.05$.